Int J Coal Sci Technol (2019) 6(2):286–300
https://doi.org/10.1007/s40789-019-0246-5

Analysis of the influence of groundwater and the stress regime on bolt behaviour in underground coal mines

Jack A. Smith[1] · Hamed Lamei Ramandi[1] · Chengguo Zhang[1] · Wendy Timms[2]

Received: 27 October 2017 / Revised: 26 March 2019 / Accepted: 3 April 2019 / Published online: 27 April 2019

Abstract The service failure of rock bolts and cable bolts are frequently reported issues in underground coal mines. Whilst numerous experimental investigations concerned with the service failure of bolts have been conducted, numerical modelling offers an alternative approach in evaluating the factors contributing to service failures of bolts in underground mines. In this study, analysis of the influence of groundwater and tensile stress on bolts in underground coal mines was studied through the numerical modelling of a grouted bolt in the immediate roadway roof. Bolt tensile stress and groundwater dripping rates in the immediate roadway roof were analysed using a package based on finite element method to assess the effect of coal roof thickness and claystone bands, as main contributors of known service failures of bolts in roadways of underground coal mines. Increasing coal roof thickness was found to increase bolt dripping rates. Probable location of stress corrosion cracking (SCC) occurrence was established through examining the shift and increase in maximum bolt tensile stress that was exhibited along the bolt length with increasing coal roof thickness. Claystone bands situated at the top and centre horizon of a grouted bolt produced lower bolt dripping rates compared with scenarios with no claystone bands. Intersecting claystone bands at the centre horizon of a bolt for a fully grouted bolt could increase the likelihood of SCC corrosion and bolt failure by contributing to microbial corrosion processes and grout fracturing by tensile stress. This study improves the understanding the bolt failure associated with the presence of groundwater and changing stress environments, which in turn is imperative in formulating strategies to mitigate support element failures and improve the ground support viability.

Keywords Numerical modelling · Groundwater · Underground coal mine · Stress corrosion cracking · Bolt corrosion · Bolt stress

1 Introduction

Grouted bolts are the primary form of roof support in underground coal mines in Australia. However, the characteristic nature of groundwater and stresses in an underground coal mine environment exposes bolts to some of the harshest conditions. Service failure of bolts due to stress corrosion cracking (SCC) and bolt–grout/grout–rock bond failure have become growing issues in underground coal mines across Australia and around the world (Cao et al. 2012; Crosky et al. 2003a; Gray 1998; Kang et al. 2013; Guo et al. 2004; Ramandi et al. 2018a; Spearing et al. 2010; Wu et al. 2018b). Understanding the factors involved in these failures is critical for developing strategies to avoid such failures.

Rock bolts and cable bolts are widely-used rock support elements that play a critical role in stabilising rock excavations. Bolts reinforce rock masses by preventing shear deformation and lateral expansion through providing shear

✉ Hamed Lamei Ramandi
h.lameiramandi@unsw.edu.au

[1] School of Minerals and Energy Resources Engineering, UNSW Sydney, Sydney, NSW 2052, Australia

[2] School of Engineering, Deakin University, Geelong, VIC 3220, Australia

resistance and axial restraining (Kang 2014; Wang et al. 2015). Windsor (1997) characterizes bolts as a reinforcement system that can be classified into three fundamental classes: Continuous Mechanically Coupled (CMC), Continuous Frictionally Coupled (CFC) and Discretely Mechanically or Frictionally Coupled (DMFC). Expansion shell bolts belong to the DMFC systems while split set and swellex bolts belong to the CFC system. CMC systems comprises of grouted bolts which could be either fully grouted or partially grouted. Partial grouted bolts assume a gap between the bolt-hole collar and the bottom of the grouted column. Because of the simple installation procedure, effective rock reinforcement and economic factors, cement or resin grouted bolts are the most commonly used ground reinforcement method (Ma et al. 2014). In Australian underground coal mines, the use of two-speed resins is currently the preferred grouting method (Vandermaat 2015). The method allows for pre-tension to be placed on the bolts, enhancing its ability to stabilise the roof rockmass (Peng 2008).

When subjected to tensile load, service failure of the bolts may occur via failure at the grout–rock interface, bolt–grout interface or in the grout medium, depending on which one is the weakest (Indraratna and Kaiser 1990a, b; Li et al. 2016). Groundwater has been found to influence failure at the grout–rock interface, partly because saturated conditions alter geomechanical properties including rock strength (Masoumi et al. 2017; Osouli and Bajestani 2016; Pan-feng et al. 2004). Together with tensile load imparted on the bolt, the reduction in rock strength reduces the effectiveness of the bolt through the degradation of bond strength between grout and rock (Osouli and Bajestani 2016). Failure at the bolt–grout interface has been found to be a result of grout splitting due to tensile stress (Tepfers 1973, 1979). Tepfers (1973, 1979) found that under tensile load, a grouted reinforcing bar will be subjected to significant stress concentrations to a point where the accumulated stresses initiate the debonding process as the stresses overcome the bonding forces (chemical adhesion, friction, mechanical interaction) at the bolt–grout interface. The debonding process is not immediate and signified by the development of splitting cracks in the grout radiating out from bolt to grout interface. The development of cracks and fractures in a grouted bolt (1) reduces the load transfer capacity of the grouted bolt and (2) facilitates the exposure of groundwater to the bolt which drives corrosion.

Roof bolts in underground coal mines are particularly susceptible to corrosion. Corrosion has been found to be responsible for 25% of all cable bolt failures and 29% of all rockbolt failures in the Australian mining industry (Potvin et al. 2001). Corrosion of bolts in roadways of an underground coal mine is primarily driven by groundwater in contact with the bolt. Numerous factors influence the rate at which bolt corrosion occurs including stress, groundwater chemical composition, microbial activity, dissolved oxygen, flow rate, pH, temperature and CO_2 content (Henthorne 1971; Spearing et al. 2010). Gray (1998) determined that the primary failure mechanism for rock bolts in service in Australian underground coal mines was due to Stress Corrosion Cracking (SCC), causing rock bolts to fail in a brittle manner at less than their recorded ultimate tensile strength. Later, Crosky et al. (2003b) reported that many of the broken bolts collected from four mine had failed from SCC. Along with Crosky et al. (2003b), studies concerned with the corrosion of rock bolts and cable bolts in underground mines has gained considerable following in recent years (Chen et al. 2018; Craig et al. 2016; Hassell 2008; Vandermaat 2015; Vandermaat et al. 2016; Wu et al. 2018a, c).

SCC is the slow progressive growth of stress corrosion cracks, which is driven by the combined influences of stress and a corrosive environment on a susceptible material, i.e. the bolts (McCafferty 2010; Vandermaat et al. 2016). Groundwater containing microorganisms that can contribute to steel corrosion has been found to play a significant role in causing SCC failure (Craig et al. 2016). Crosky et al. (2002) found that SCC in bolts was more prevalent in underground coal mines with thick coal roofs, saturated roof strata, and the presence of claystone or tuffaceous bands within the bolting horizon. In-hole coupon bolt tests by Craig et al. (2016) also confirmed intersecting claystone bands as a major contributor to bolt corrosion.

Considering the difficulty and cost of site monitoring, numerical modelling offers an alternative approach to evaluating key factors contributing to service failures of bolts in underground mines. Whilst there has been substantial numerical modelling studies of stress distribution and deformation of bolts in roadways of underground mines, the numerical modelling of bolts in underground roadways focusing on both stresses and groundwater has received little to no attention. Furthermore, to date, studies concerned with bolt corrosion and SCC failure of bolts in underground coal mines has remained largely experimental (Aziz et al. 2014; Craig et al. 2016; Vandermaat 2015; Vandermaat et al. 2016; Wu et al. 2018a, c).

Herein, numerical methods are used to assess the effect of coal roof thickness and claystone bands as factors contributing to known service failures of bolts in roadways of underground coal mines. Several conditions that may exist in an underground mine are designed to model bolt tensile stress and groundwater discharge flow rates in the immediate roadway roof of the bolting region. Then the parameters involve in the bolt failure are quantified to evaluate the likeness of bolt failure.

2 Numerical modelling methods for ground support and groundwater interactions

A wide range of numerical methods such as finite element method (FEM), boundary element method, discrete element method, finite difference method (FDM) and the hybrid method can be employed to conduct stress and groundwater analysis in geomechanics (Liu et al. 2016; Zhang et al. 2012). The most common methods employed in the numerical modelling of ground support and groundwater interactions in underground coal mines are the FDM and FEM (Anderson et al. 2015), in cases where the rock mass behaviour in the area of interest is not significantly controlled by high-density discontinuities and the interaction with support elements.

FDM is based on the discretization of governing partial difference equations (PDE's) in problem regions with simple boundaries (Zhang et al. 2012). The use of FDM is well represented in numerous studies concerned with modelling of ground support in underground mines (Ma et al. 2014; Nemcik et al. 2014). Ma et al. (2014), simulated the fully grouted rock bolt in underground roadways using FLAC2D. The study recognised that although rock support elements provided by numerical modelling software are widely used for modelling bolts in the field, they do not feature the interfacial shear bond between bolt, grout and rock, i.e. modelling the bolt–grout as a single element material. To model the non-linear bond slip relationship between bolt–grout–rock, established by Nemcik et al. (2014) and Ma et al. (2014) used FISH (a programme language embedded within FLAC) to modify the bolt elements to accommodate the non-linear bond slip relationship between bolt–grout–rock. For groundwater modelling, FDM is the most commonly used numerical method for solving groundwater flow problems (Anderson et al. 2015). The modelling of groundwater interaction in underground coal mines using the FDM has seen considerable focus in recent years (Light and Donovan 2015; Newman et al. 2017; Nguyen et al. 2014; Surinaidu et al. 2014). Surinaidu et al. (2014) focused on the hydrogeological and groundwater modelling of groundwater inflows into an underground coal mine in India using a finite difference code MODFLOW. Similarly, Nguyen et al. (2014) used FLAC to study the influence of water inrush on underground coal mining stability in Vietnam in order to estimate when mining activity should pause and handling of water inrush should take place. FDM is simple and well suited for material non-linearity. However, as highlighted by Zhang et al. (2012), regular quadrilateral mesh systems within FDM models limits its application in terms of the description of complex boundary conditions.

FEM involves solving a system of equations based on the displacement of finite elements specified by a fixed number of nodes in a discretised domain. Figure 1 demonstrates a finite element mesh; combination of nodes and elements. By determining the node displacements, stresses and strains in each element throughout the mesh are then obtained. Notable software packages which employ the FEM for studying ground support include ANSYS, ABAQUS and RS^2 ($Phase^2$ 9.0). Several studies have adopted FEM in the modelling of bolts in underground mines (Jalalifar and Aziz 2012; Yassien 2003). Yassien (2003) studied two-dimensional numerical simulation and design of fully grouted bolts for underground coal mines in the United States. Using ABAQUS 5.8, finite element models were developed to simulate the components of a fully grouted bolt and its interaction with surrounding roof strata. Jalalifar and Aziz (2012), using the 3D finite element software ANSYS, simulated the fully grouted bolt under lateral and axial loading. Adhikary and Wilkins (2012) used FEM to model groundwater interactions in an underground coal mine. They evaluated the impact of longwall extraction on groundwater systems as part of a research project carried out under the Australian Coal Industry's Research Program (ACARP). The study involved monitoring of mine water and groundwater conditions and development of a hydro-geomechanical model using the CSIRO proprietary finite element code COSFLOW, although model predictions are yet to be compared to observations of near-surface effects. Popularity of the

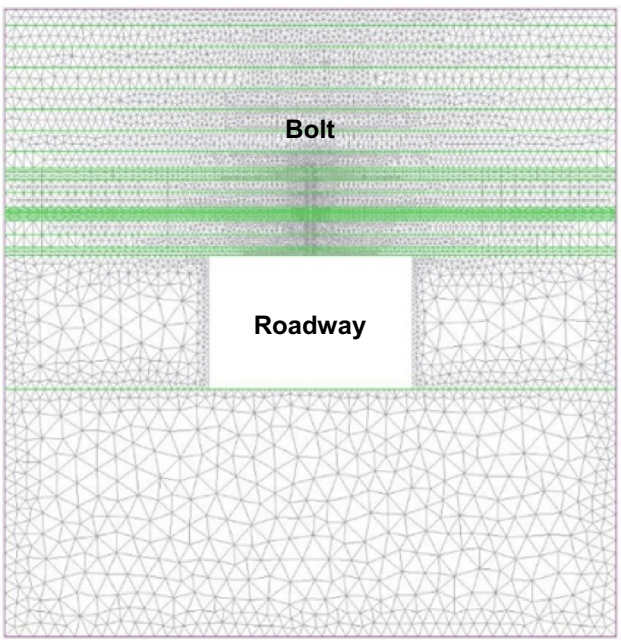

Fig. 1 Finite element mesh with RS^2. Green lines represent material boundaries used to differentiate various stratigraphic layers used in this study

finite difference code MODFLOW and restrictions on the proprietary finite element codes FEFLOW and COSFLOW, has contributed to the limited adoption of these codes, and coupled geomechanical-groundwater models for underground coal mines. Nonetheless, compared to the FDM, FEM is well suited to irregularly shaped boundaries, internal heterogeneities, sinks and sources and complex features such as fault zones (Anderson et al. 2015). FEM is also relatively flexible in dealing with non-linear coupled processes, material inhomogeneity, anisotropy, and complex boundary conditions (Zhang et al. 2012). For these reasons, along with findings from Ma et al. (2014), a finite element modelling method was adopted in this study.

3 Model methodology

Groundwater discharge flow rates and bolt tensile stresses in a roadway of an underground coal mine was analysed using a FEM code, RS^2 ($Phase^2$ 9.02), in this study. RS^2 ($Phase^2$ 9.02) is a two-dimensional implicit FEM software code developed by Rocscience Inc. for soil and rock applications (Rocscience Inc. 2017). The software includes steady-state, finite element groundwater seepage analysis to which pore pressure, flow and gradient can be determined along with effective stress. The software has been previously adopted to perform numerical modelling in numerous studies (Coggan et al. 2012; Coli et al. 2008; Day et al. 2017; Grenon et al. 2017; Perras and Diederichs 2007; Sasaoka et al. 2016; Smith 2016; Winn et al. 2017; Zsaki 2010). RS^2 ($Phase^2$ 9.02) was selected for the study given finite element capability, user friendly interface and relatively simple application.

The models were developed based on hydrological and geological conditions from Mine A, an underground longwall coal mine situated in the Western Coalfields of New South Wales, Australia. Mine A is a relatively wet mine extracting coal from the Lithgow Seam which lies in upper Permian Illawarra Coal Measures dominated by fluvial sandstones and floodplain siltstones (Adhikary and Wilkins 2012). Major rock types present at Mine A include a bituminous coal locally known as "Lithgow coal", along with sandstones and siltstones with tuffaceous claystone bands. Mining occurs at a depth of 350–380 m with the extraction of a 3.2 m section of the 7 m Lithgow coal seam (Adhikary and Wilkins 2012). Typical roof lithology at Mine A consists of a 3–4 m thick coal roof with two 100–200 mm claystone bands situated within the bottom 1.2 m horizon (Craig and Murnane 2013). The mine groundwater specifications are provided in Table 1 (Mine A) in Wu et al. (2018d).

A plane strain analysis is implemented where two principal in situ stresses are in the plane of the excavation and the third principal stress is out of plane. Out of plane strain is assumed to be zero in the analysis. For the stress analysis, an implicit FEM based on the finite element formulations described by Owen and Hinton (1980) and Chen (1982) were used. Matrices representing the system of finite element equations was solved using Gaussian Elimination. Steady state groundwater seepage analysis are based on fluid flow equations described by Fredlund and Rahardjo (1993). A pore fluid unit weight of 0.00981 MN/m^3 was assumed. As demonstrated in Fig. 2, a graded mesh using 3 noded triangles consisting of approximately 17,000 elements was used. The mesh was optimised using advanced meshing regions to reduce computational time. Computations were performed on a local computer with a 3.00 GHz CPU and 8.00 GB RAM using Version 9.02 of the RS^2 ($Phase^2$ 9.02) software code. Each model had a run time of around 8 min.

3.1 Model setup

A single 22 mm diameter plain strand HSAC 840 grouted rock bolt with a length of 2.1 m, which is widely used in Australian mining industry, was modelled in an underground coal mine roadway (3 m × 5 m). Figure 2 demonstrates a model used in this study, where the bolt is installed in the centre of the roof to represent the tensile failure scenario. Partially grouted and fully grouted bolts were considered with grouting filling a 6 mm thickness annulus to the bolt. Partially grouted bolts were modelled with a gap of 0.5 m between the bolt-hole collar and the bottom of the grouted column. Bolt groundwater flow rates were measured using discharge sections over a distance encompassing the bolt and grout annulus; bolting region. The bolting region is demonstrated in the insets in Fig. 2. Bolt tensile stresses were measured along the centreline over the entire 2.1 m length of the bolt. Note that due to the difficulty in conducting field measurements and obtaining hydrogeological and geological parameters inherent to Mine A, many model parameters used in this study were based on previous works, in particular Adhikary and Wilkins (2012).

3.1.1 Boundary conditions

Hydraulic boundary conditions were specified for the external and excavation (roadway) boundaries. Adhikary and Wilkins (2012) reported a total hydraulic head of 120 m at the coal extraction level for Mine A. As seen in Fig. 2b, a total hydraulic head of 120 m was assumed for left boundary of the model. The top and bottom boundaries were assumed as no flow boundaries and the roadway and right boundary were set as seepage face boundaries which allowed for seepage.

Table 1 Material and hydraulic properties used in models (Adapted from Adhikary and Wilkins (2012))

Material	Material properties								Hydraulic properties	
	E (GPa)	v	UTS (MPa)	ϕ' (°)	c′ (MPa)	σ_c (MPa)	m_b	s	K ($K1$) (m/s)	$K1$/$K2$
Lithgow coal	4.5	0.3	0.5	40	1.3				2.57E−8	1.5
Claystone	8	0.3	0.77	35	2				8.58E−10	4
Sandstone	15	0.3	1.5	35	4				8.58E−9	10
Siltstone	10	0.3	1.15	35	3				8.58E−9	10
Bolt	200	0.3	840	45	500				1E−20	1
Grout	2.88	0.3				80	3	1	1.6E−12	1

Major and minor horizontal in situ stresses at Mine A were 15 MPa and 12 MPa, respectively (Adhikary and Wilkins 2012). As demonstrated by Hoek and Brown (1980), vertical stress can be estimated by:

$$\sigma_v = 0.027z \quad (1)$$

where z is the depth below the surface. Worldwide data on measured in situ rock stress analysed by Hoek and Brown (1980) found that the average unit weight of rock is typically about 0.027 MN/m^3 which is reflected in Eq. (1). Using Eq. (1), vertical stress was estimated to be 10 MPa at the coal extraction level depth for Mine A. In-plane major and minor stresses were 15 MPa and 10 MPa, respectively, with a major stress angle of 0° to the horizontal x-axis.

3.1.2 Material properties

Material properties of the stratigraphic units used in this study are typical of Mine A and are unmodified to values used by Adhikary and Wilkins (2012). The set of material properties used in the models are listed in Table 1. Materials were defined as elastic and isotropic with a single Young's Modulus (E) and Poisson's ratio (v). The Mohr–Coulomb failure criterion was used to define the strength criteria of stratigraphic units in this study. The Mohr–Coulomb Criterion assumes that rock failure occurs as a result of shear displacement along a shear surface cutting through intact rock. Considering pore pressure, shear failure is predicted to occur when the shear stress on a particular surface exceeds the shear strength (τ_f) of an intact rock, which is given by (Heyman 1972):

$$\tau_f = \sigma'_n \tan\phi' + c' \quad (2)$$

where σ'_n is the effective normal stress, ϕ' is the effective friction angle and c' is the effective cohesion. The parameters ϕ' and c' in Eq. (2) are inherent material properties which define the strength envelope of a material.

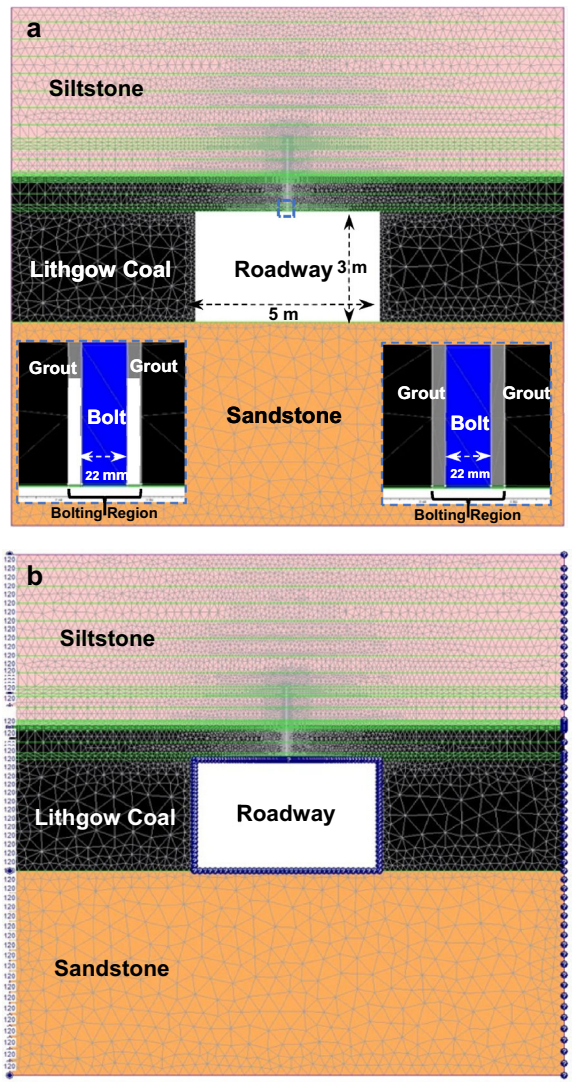

Fig. 2 A model layout used in this study designed using RS^2. **a** inset left and right is an example of a partially grouted and fully grouted bolt, respectively, **b** model layout demonstrating hydraulic boundary conditions. Note left hand boundary of 120 m hydraulic head

Intrinsic to the Mohr–Coloumb strength criteria, ultimate tensile strength (*UTS*) for materials was also specified.

Grout properties were based on a high strength thixotropic grout. Grout/resin material properties assumed the Hoek–Brown failure criterion. The Hoek–Brown criterion is an empirical failure criterion defined in terms of biaxial principal failure stress, σ_1 and σ_3, and the uniaxial compressive strength, σ_c. For a rock mass, the Hoek–Brown failure criterion is given by:

$$\sigma_1 = \sigma_3 + \sigma_{ci}\left(m_b \frac{\sigma_3}{\sigma_{ci}} + s\right)^{0.5} \quad (3)$$

where m_b is the material constant for rock mass (varies with rock type) and s is a curve fitting constant. Grout σ_c was based on a HS400 txotropic grout at water/cement ratio of 0.35. Given a water/cement ratio of 0.35, Hoek–Brown parameters in Eq. (3), m_b and s, were then estimated [after Hyett et al. (1992)]. Bolt properties were in accordance to a typical 22 mm diameter HSAC 840 plain strand rebar bolt with an ultimate tensile strength of 840 MPa. Further details pertaining to bolt properties are discussed in Sect. 3.1.4.

3.1.3 Hydraulic properties

The permeability of a rock mainly depends on its pore space properties, i.e. porosity, pore size distribution, connectivity, fracture dimensions, fracture density and degree of mineralization (Jing et al. 2017; Mostaghimi et al. 2016; Pittman 1992; Ramandi et al. 2016, 2018b; Snow 1968; Wong et al. 1984). It also can be a highly non-linear dynamic function of mining induced stress and subsequent fractures (Adhikary and Wilkins 2012; Guo and Yuan 2015; Guo et al. 2012; Kelsall et al. 1984; Wang and Park 2002). Therefore, it is not only important to estimate the rock permeability but consider the possible variations in permeability induced by mining activity. Hydraulic conductivities of stratigraphic units used in this study are listed in Table 1. Grout hydraulic properties used in this study was based on research by Allan (1999) and listed in Table 1. Suitability of the grout hydraulic conductivity was assessed and confirmed via the agreement of modelled results with observed results as highlighted in Sect. 4.1. Bolt hydraulic conductivity assumed the lowest permissible non-zero value (1×10^{-20} m/s) to ensure numerical stability. $K1/K2$ in Table 1 is a ratio of horizontal hydraulic conductivity to vertical hydraulic conductivity where $K1$ is the primary hydraulic conductivity (horizontal hydraulic conductivity).

3.1.4 Bolt–grout design

The complexity in the numerical simulation of grouted bolts has been facilitated by numerical models that readily accommodate a variety of supporting systems including different bolting types. However, many of the bolting types found across a wide range of numerical modelling software packages lack the detail that is sometimes required for numerical analysis. In this study, the bolt and resin/grout were modelled as separate materials with their own inherent material and hydraulic properties as listed in Table 1. This can serve for evaluating the variation in bolt tensile stresses due to coal roof thickness and intersecting claystone bands. As such, the steel HSAC 840 bolt can effectively be modelled as an equivalent material adhering to the Mohr–Coulomb failure criterion, provided that stresses do not exceed the strength envelope of the equivalent bolt material. Bolt properties used in this study are presented in Table 1.

3.2 Model scenarios

All models used in this study possessed the same model dimensions, model geometry, mesh configuration and number of mesh elements. The study focused on two model scenarios: (1) varying coal roof thickness and (2) varying claystone band configurations. Two separate Base Models were developed for each scenario: Coal Roof Base Model (CRBM) and Claystone Band Base Model (CBBM). Coupled with their Base Models, numerous iterations of either variation in coal roof thickness or claystone band configuration was conducted in order to assess their influence on groundwater discharge flow and bolt tensile stress. A total of 12 iterations of Scenario 1 were designed and modelled: 0.1 m (Coal Roof Base Model), 0.2 m, and 0.5–5 m (0.5 m increments). Figure 2 demonstrates a model iteration from Scenario 1 with a coal roof thickness of 1 m. CRBM had a sandstone roadway base, Lithgow coal roadway ribs and a 0.1 m Lithgow coal roadway roof with the remaining roof being siltstone.

A total of 18 iterations of Scenario 2 were designed and modelled to represent varying claystone band: thickness (100–300 mm), position along the bolt length (top–centre–collar) and frequency. Table 2 lists the 18 model iterations of Scenario 2 along with their respective claystone band configuration in terms of thickness and position. The CBBM was made up of a sandstone roadway base, coal roadway ribs and no claystone bands within a 4 m coal roof (with the remaining 1 m above being siltstone). The 4 m coal roof thickness was maintained throughout the 18 iterations of Scenario 2 to solely assess the impact of claystone bands variations on groundwater discharge flow rates and bolt tensile stresses. Scenario 1 and 2 were

Table 2 Model iterations of Scenario 2—varying claystone band configurations

Model name	Configuration and thickness (mm)		
	Top	Centre	Collar
CBBM	0	0	0
1	0	0	100
2	0	0	200
3	0	100	0
4	0	200	0
5	0	300	0
6	100	0	0
7	200	0	0
8	300	0	0
9	100	0	100
10	200	0	200
11	100	100	0
12	200	200	0
13	300	300	0
14	0	100	100
15	0	200	200
16	100	100	100
17	200	200	200

applied to both fully grouted and partially grouted bolts, and thus a total of 60 model iterations were conducted in this study.

4 Model validation

4.1 Model verification: Mine A

The verification of the model was conducted using bolt groundwater flow rates and bolt tensile stress data obtained from previous works conducted at Mine A (Craig et al. 2016; Hebblewhite and Lu 2004; Vandermaat 2015). Bolt drip rates due to groundwater flow from Mine A were reported by Craig et al. (2016). Groundwater flow rate data was obtained through inspecting 1062 bolts in roadways of Mine A. Of the 1062 bolts, 206 bolts were found to be dripping. The average discharge rate for these bolts was 9.5 mL/min with a standard deviation of 46.5 mL/min. Table 3 lists some key statistics pertaining to the groundwater discharge flow rates observed by Craig et al. (2016) and groundwater discharge flow rate averages for various groupings of modelled results. Figure 3 graphically demonstrates modelled results versus observed results. Comparing modelled discharge flow rates and observed discharge flow rates it can be concluded that all modelled

Table 3 Statistics of observed groundwater discharge flow rates after Craig et al. (2016) and modelled results

Modelled results	
Scenarios	Average discharge (mL/min)
Scenario 1—fully grouted bolts	8.89E−06
Scenario 2—fully grouted bolts	1.25E−04
Scenario 1—partially grouted bolts	4.95
Scenario 2—partially grouted bolts	13.26
Scenario 1—all bolts	2.48
Fully grouted bolts	7.62E−05
Partially grouted bolts	9.78
Observed results	
Total number of bolts	1062
Number of bolts dripping	206
Percentage of bolts dripping	19.4%
All bolts	
Average	9.45 mL/min
Standard deviation	46.5 mL/min
Maximum	1100 mL/min
Median	0 mL/min
Minimum	0 mL/min
Mode	0 mL/min
Dripping bolts	
Average	48.7 mL/min
Standard deviation	96.1 mL/min
Maximum	1100 mL/min
Median	20 mL/min
Minimum	2.5 mL/min
Mode	10 mL/min

results lie within the range of observed results. Figure 3 suggests that partially grouted bolts amongst both model scenarios are in the best agreement with observed results, for base case hydraulic conductivity values. Comparison of averages in Fig. 3, further suggests that partially grouted bolts best suit the observed results with a modelled groundwater discharge flow rate average of 9.78 mL/min in comparison to observed results average for all bolts of 9.45 mL/min. This is because partially grouted bolts can be seen to represent a variety of in situ bolt occurrences which readily arise in the field. This includes partially grouted bolts, bolts that have been improperly grouted, and bolts where grout erosion has occurred. The relatively high maximum observed flow of 1100 mL/min was measured at a cut-through which, as Craig et al. (2016) highlights, coincides with the proximity of abandoned and flooded mine workings.

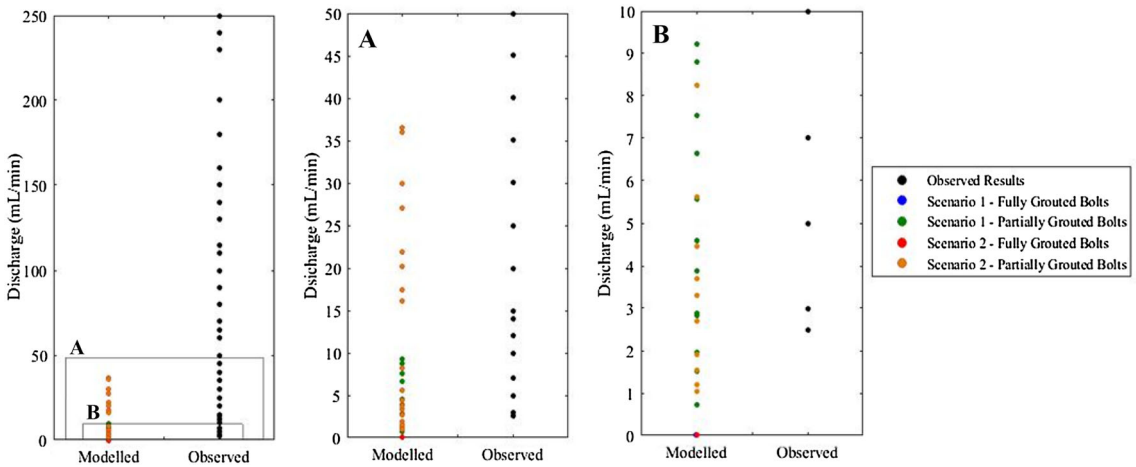

Fig. 3 Modelled versus observed groundwater discharge flow. Modelled partial grouted bolts for both Scenario 1 and 2 (base case hydraulic conductivity values) agree best with observed results

Maximum bolt tensile stress data from Mine A was obtained from previous work by Hebblewhite and Lu (2004). Bolt tensile stress data was acquired through performing strain-gauge bolt tests using instrumented bolts as part of a study to understand roof deformation behaviour and the performance of rock bolting reinforcement in laminated, weak coal mine roof strata. Six instrumented bolts were installed to study roof deformation behaviour of Mine A. Figure 4 demonstrates the maximum bolt tensile stress data for the six instrumented bolts superimposed against the maximum bolt tensile stress data for all 60 numerical models used in this study. As Fig. 4 shows the modelled maximum bolt tensile stresses are well represented by 4 out of the 6 instrumented bolts (Bolts 2,3,4 and 6) used in Mine A.

.

4.2 Sensitivity analysis

A sensitivity analysis was conducted to study model input parameter sensitivity to the model results. Groundwater discharge flow rates and bolt tensile stresses (model results) were recorded for each sensitivity model scenario to identify which of the model parameters are the most influential on bolt groundwater discharge rates and bolt tensile stresses. Sensitivity analysis was conducted on (1) hydraulic conductivity of stratigraphic units and grout, (2) total hydraulic head, and (3) field stress.

Sensitivity of the model results to the variation in hydraulic conductivity was assessed by multiplying hydraulic conductivities by factors of 0.1 (decrease) and 10 (increase). Similarly, sensitivity of the model results to the variation in total hydraulic head and field stress is assessed by multiplying total hydraulic head and field stress by

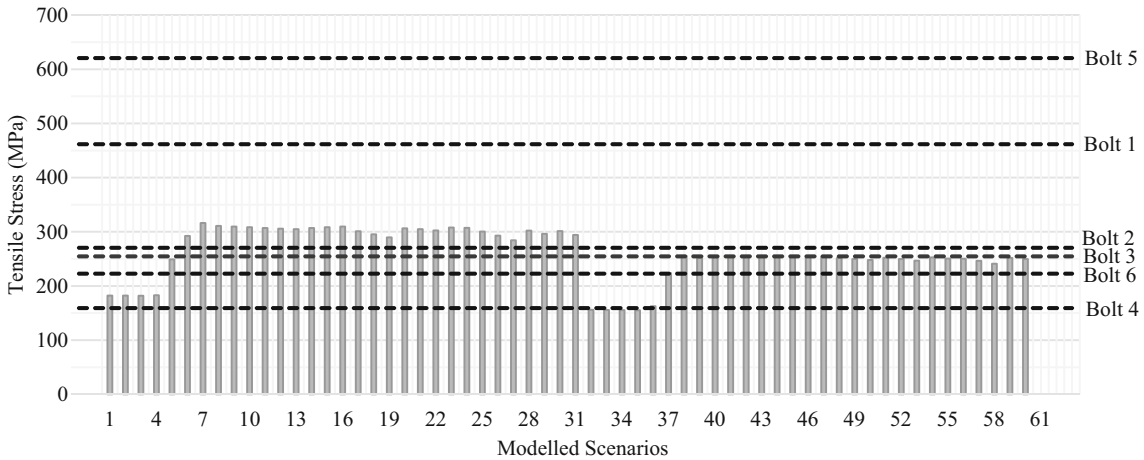

Fig. 4 Maximum bolt tensile stress from previous work by Hebblewhite and Lu (2004) superimposed against maximum bolt tensile stress data for all 60 modelled iterations. Modelled results are well represented by bolts 2, 3, 4 and 6

factors of 0.5, 1.5 and 2. Results of the sensitivity analysis can be seen in Table 4.

As shown in Table 4, model parameters, notably, hydraulic conductivity and total hydraulic head, do not have statistically significant effects on tensile stress exhibited on the bolt. As expected, bolt tensile stress was found to be sensitive to variations in field stress with a factor of two increase and halving resulting in a 100% and − 50% change in bolt tensile stresses, respectively.

Groundwater discharge flow rates is found to be very sensitive to hydraulic conductivity of some stratigraphic units and grout, and total hydraulic head. Sensitivity of groundwater discharge results to hydraulic total head showed a near linear relationship with a multiplication factor of 0.5, 1,5 and 2 resulting in a − 53%, 53% and 107% change in groundwater discharge flow rate, respectively. The model was sensitive to the hydraulic conductivity of the grout since an order of magnitude increase resulted in a 903% increase in groundwater discharge flow rate. This may prove significant in the context of grout fracturing which (1) readily occurs in bolt installations underground and (2) facilitates the exposure of groundwater to the bolt which could lead to corrosion. This finding suggests that mitigating the fracturing of grout during installation of bolts, and partial loss of grout from the annulus near the mine roof, could be important to reduce exposure to groundwater, and thus SCC failure of bolts.

5 Results and discussion

5.1 The effects of coal roof thickness

Figure 5 shows the effects of coal roof thickness on groundwater discharge flow rates. Groundwater flow rates were significantly higher in bolts with partial grouting as oppose to fully encapsulated bolts as Fig. 5 indicates. For fully grouted bolt, increasing coal roof thickness led to an increase in bolt groundwater dripping rates in the underground roadway roof. Figure 6 is an RS^2 output demonstrating pore pressure contours and groundwater flow lines for fully grouted bolts with increasing coal roof thickness.

Note the changes in pore pressure and groundwater flow direction around the bolt installation with increasing coal roof thickness. For partially grouted bolts, bolt dripping rates increased as the coal roof thickness increased from 0.5 to 5 m. Decrease in bolt dripping rates from the Base Model (0.1 m) to 0.5 m for the partially grouted bolt may be attributable to the 0.5 m un-grouted gap between the bolt-hole collar and the start of the grouted column.

The increasing groundwater discharge flow rate associated with increasing coal thickness would influence the rate at which bolt corrosion would occur through simultaneously increasing the rate at which dissolved corrosive media come into contact with the bolt (Henthorne 1971), providing sources for other constituents involved in corrosion (e.g. microbes, sulphate), and flushing away corrosion reaction products, thus increasing reaction rates

Table 4 Sensitivity analysis results

Item	Factor	Discharge (mL/min)	Discharge change (%)	Bolt tensile stress (MPa)	Bolt tensile stress change (%)
Base model, no variation		3.763E−06	–	301.78	–
Sandstone *K*	10	3.772E−06	0	301.78	0
	0.1	3.761E−06	0	301.78	0
Lithgow coal *K*	10	6.615E−07	− 82	301.88	0
	0.1	1.180E−05	213	301.58	0
Siltstone *K*	10	3.952E−06	5	301.81	0
	0.1	3.718E−06	− 1	301.77	0
Claystone *K*	10	9.500E−06	152	301.52	0
	0.1	6.641E−07	− 82	301.88	0
Grout *K*	10	3.775E−05	903	301.78	0
	0.1	3.762E−07	− 90	301.78	0
Hydraulic total head	0.5	1.757E−06	− 53	301.54	0
	1.5	5.770E−06	53	302.02	0
	2	7.778E−06	107	302.25	0
In-situ field stress (σ_1, σ_2, σ_3)	0.5	3.763E−06	0	151.11	− 50
	1.5	3.763E−06	0	452.45	50
	2	3.763E−06	0	603.12	100

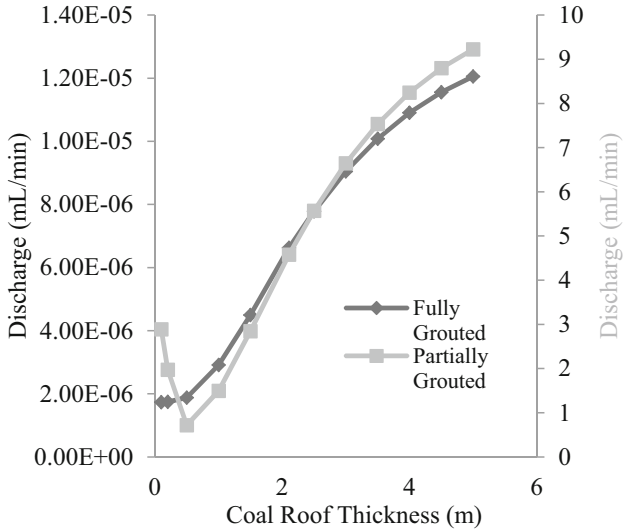

Fig. 5 Effects of coal roof thickness on groundwater discharge flow rates for fully grouted (dark) and partially grouted (light) bolts

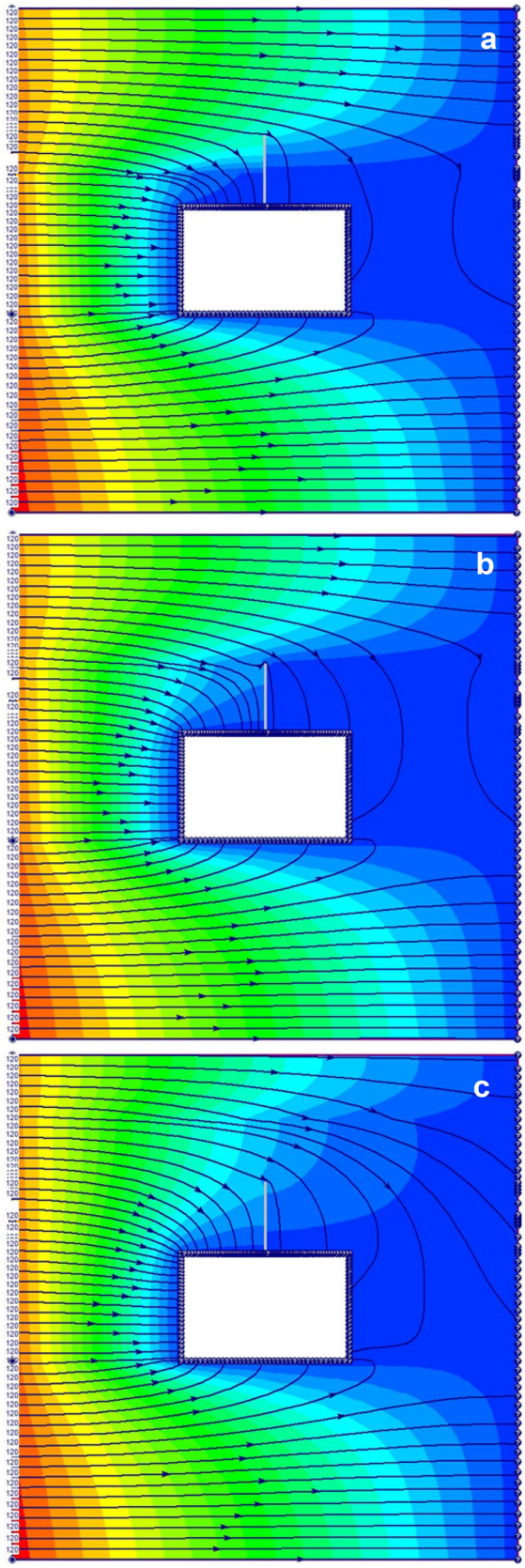

further. The rate of bolt corrosion has been found to be largely influenced by concentration of dissolved oxygen in groundwater. As such, increasing groundwater discharge flow rates associated with increasing coal roof thickness, coupled with a tensile load, could lead to bolt SCC failure. In addition, it can significantly impact the bolt–grout/grout–rock bond.

Maximum tensile stress along the bolt increased as coal roof thickness increased up to the length of the bolt (2.1 m). Highest bolt maximum tensile stress was seen at a coal roof thickness that was equivalent to the 2.1 m bolt length for both fully encapsulated and partially grouted bolts. Compared to the CRBM, maximum bolt tensile stress increased by 73% for the fully encapsulated bolt and 64% for the partially grouted bolt as coal roof thickness reached 2.1 m (length of the bolt). Similar findings were noted by Coggan et al. (2012), who showed that the extent of the failure zone in a road way is controlled by the thickness of weak immediate roof lithology. This increased failure zone would correlate to increased roof deformation which would reflect an increase in bolt tensile load and maximum tensile stress exhibited on the bolt.

Figure 7 illustrates bolt tensile stress distribution over the entire 2.1 m bolt length for a fully encapsulated bolt at various coal roof thicknesses. Figure 7 clearly highlights the shift in where the maximum tensile stress is exhibited along the bolt with increasing coal roof thickness (up to the length of the bolt). This result may prove useful in pinpointing the location along a given bolt length to where bolt SCC failure would likely occur. A similar result was noted for the partially grouted bolt. The fully encapsulated bolt exhibited a higher maximum tensile strength

◀**Fig. 6** RS^2 schematic pore pressure output with flow lines for fully grouted bolts at various coal roof thickness. **a** 1 m, **b** 2.1 m (bolt length), and **c** 5 m

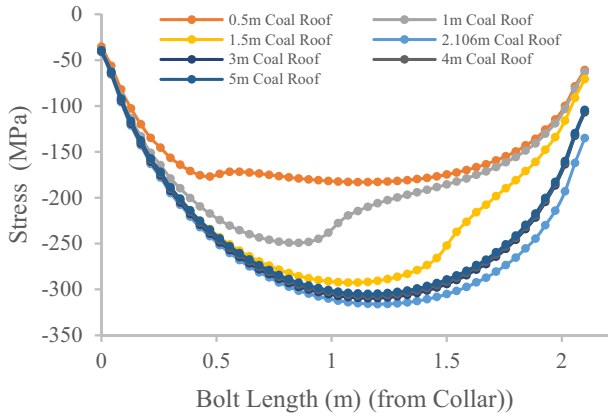

Fig. 7 Stress distribution along 2.1 m fully grouted 22 mm HSAC 840 steel bolt with increasing coal roof thickness

consistently in comparison to the partially grouted bolt independent of coal roof thickness.

5.2 The effects of claystone bands

Seventeen claystone band configurations, varying in thickness (100–300 mm), position along the bolt length (top–centre–bottom) and frequency were modelled in Scenario 2 to assess the effect of claystone bands on bolt maximum tensile stresses and groundwater discharge flow rates. The results are presented in Fig. 8. Relatively high groundwater flow rates were modelled in claystone bands configurations that had (1) thin claystone bands, (2) the fewest claystone bands and (3) claystone bands situated at

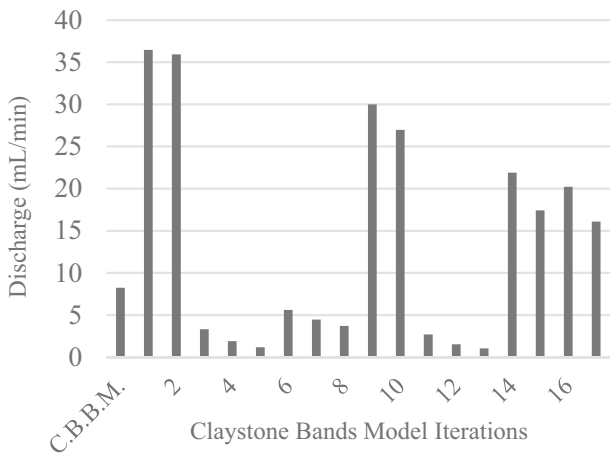

Fig. 8 Partially grouted bolt discharge flow rates for 17 clay band model iterations. C.B.B.M. represents *Clay Band Base Model.* Description of Clay Band models is listed in Table 2

the immediate roof of the roadway (closest to bolt-hole collar). The claystone band configuration bearing a single 100 mm (thinnest) claystone band situated at the immediate coal roof (collar) resulted in the highest groundwater flow discharge rate out of the bolting region for all the modelled flow rates (Table 3). This was prevalent in both the fully encapsulated and partially grouted bolt conditions. The Base Model (no claystone bands) yielded a higher discharge flow rate than claystone band configurations that did not have claystone bands situated at the immediate coal roof as seen in Fig. 8. This indicates that having claystone bands at the top and centre horizon of the bolt produces lower groundwater discharge flow rates than having no claystone bands at all. These results are attributable to the lower permeability of claystone and intrinsic ability to retain moisture, thus maintaining groundwater contact with the bolt within and above the claystone band. Craig et al. (2016) observed such effects whilst conducting in-hole rock bolt corrosion coupon testing for Mine A. They found that after 128 days of persistent bolt dripping in the installed in-hole rock bolt corrosion coupon, dripping had ceased. Upon removal of the coupon, the top of the coupon contained puggy clay material and approximately 500 mL of groundwater above the clay plug which explained why dripping ceased over time. In regards to the service failure of bolts, studies concerned with microbial corrosion of steel have shown that clay/claystone possess sufficient nutrients and trace elements for the growth of microorganisms such as sulfate-reducing bacteria (SRB) (El Hajj et al. 2010). SRB is known to be corrosive towards metals, including steel. This may suggest that although claystone bands bearing the thickest claystone bands produced comparably lower groundwater discharge flow rates, they may in fact play an equally significant role in contributing to corrosion; and combined with tensile stress, SCC failure.

Maximum bolt tensile stresses for the 18 claystone band configurations remained relatively similar. Claystone bands situated in the centre of the bolt length appeared to be the greatest contributing factor in effecting maximum tensile stress in the bolt. Claystone band configurations with claystone bands situated in the centre horizon of the bolt length had consistently lower maximum bolt tensile stresses. Furthermore, as claystone band thickness increased in this centre horizon of the bolt length, maximum bolt tensile stresses decreased. Highest maximum bolt tensile stress was observed in claystone band configurations that had (1) thin claystone bands, (2) no claystone bands in the centre horizon of bolt length and (3) claystone bands situated at the immediate roof of the roadway.

Model configurations with claystone bands situated at the immediate roof or the roadway and with no claystone bands in the centre of the bolt produced maximum bolt tensile stress results that were higher than the CBBM

results. All remaining claystone band configurations appeared to reduce the maximum bolt tensile stress compared to the CBBM configuration.

Fully grouted bolts for the various claystone band configurations produced maximum bolt tensile results that were consistently higher than partially grouted bolts with increases varying between 16% and 22%. This is expected and conforms to the load transfer concept described by Windsor (1997). The longer anchorage length associated with a fully grouted bolt allows the transfer of more load which therefore induces more stress on the bolt. The shorter anchor length associated with partially grouted bolts limits the transfer of load which is indicative to the 16% and 22% difference between maximum tensile stress for the fully and partially grouted bolt. Figure 9 suggests that maximum tensile stress for a fully and partial grouted bolt is found at the centre of the length of the grouted column.

For the fully grouted condition, highest tensile stress is exhibited at the centre along the length of the bolt installation. Grout splitting and fracturing in the grout annulus at the centre along the bolt length would be more likely to occur in this region. Given the influence of claystone in contributing to microbial corrosion of steel bolt (El Hajj et al. 2010), having grout fractures in this region would present highly unfavourable conditions and significantly increase the likeliness of bolt corrosion and SCC failure. This indicates that intersecting claystone bands at the centre horizon of the bolt length for a fully grouted bolt may increase the likeliness of SCC bolt failure to occur.

For the partially grouted condition, the maximum tensile stress is exhibited at the centre of the length of the grouted column, or 1.3 m from the bolt-hole collar of the 2.1 m bolt. The region of maximum tensile stress and potential

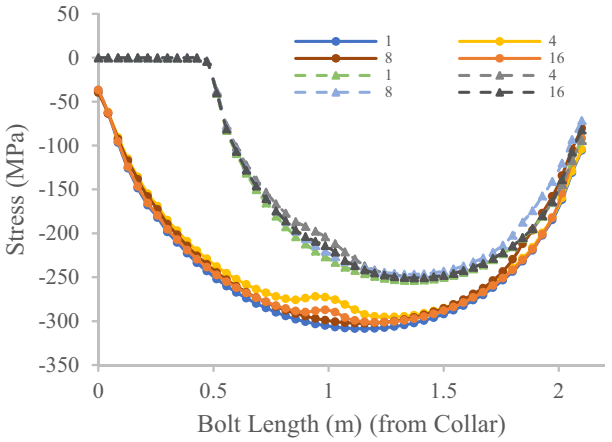

Fig. 9 Stress distribution along 2.1 m fully grouted (circle-solid line) and partially grouted (triangle-dash line) HSAC840 steel bolt for a selected number of clay band iterations. Description of Clay Band models is listed in Table 2

grout splitting and fracturing is situated in an exclusive region in between the top and centre of the bolt length where, in this study, there are no intersecting claystone bands. Whilst this may reduce the effects of bolt corrosion and SCC failure, the likely occurrence of an increase in field stresses due to ground movement would initiate more grout splitting and fracturing. This would increase prevalence of the fractured grouted region in the grouted column to which it may eventually overlap an area of the bolt with intersecting claystone bands. In any case, in the interest of minimising bolt corrosion and SCC failure, the choice of fully grouted or partially grouted bolts is largely influenced by lithology of the roof of the underground roadway.

6 Conclusions

Analysis of the influence of groundwater and tensile stress on bolts in underground coal mines was performed via the numerical modelling of a grouted bolt in the immediate roadway roof of an underground coal mine. Bolt tensile stress and bolt groundwater dripping rates in the immediate roadway roof was analysed using the FEM code, RS^2 ($Phase^2$ 9.02) to assess the effect of coal roof thickness and claystone bands as main contributors of corrosion, SCC failure and bolt–grout/grout–rock bond failure of bolts in roadways of underground coal mines. It was shown that increasing coal roof thickness can lead to an increase in bolt discharge flow rates. The increase groundwater flow towards drips would simultaneously increase reaction rates (e.g. dissolved oxygen supply) leading to SCC bolt failure, particularly if tensile stress is also significant. The sources of groundwater flow and constituents involved in microbial and corrosion processes beyond the adjacent coal roof are less certain. It was observed that maximum tensile stress along the bolt increased as coal roof thickness increased up to the length of the bolt (2.1 m). Probable location of SCC occurrence was established through examining the shift and increase in maximum bolt tensile stress that is exhibited along the bolt length with increasing coal roof thickness. For the fully grouted bolt, intersecting claystone bands at the centre horizon of the bolt length may increase the likeliness of SCC bolt failure to occur given the influence of claystone in contributing to microbial corrosion of the steel bolt, together with the development of grout splitting and fracture given the high tensile stress habitual to this region along the length of the bolt. Highest maximum bolt tensile stress was observed in claystone band configurations that had (1) thin claystone bands, (2) no claystone bands in the centre horizon of bolt length and (3) claystone bands situated at the immediate roof of the roadway. Highest groundwater discharge flow rates out of the bolting region were observed in claystone bands

configurations that had (1) thin claystone bands, (2) the fewest claystone bands and (3) claystone bands situated at the immediate roof of the roadway. Mitigating the fracturing of grout during installation of bolts, and partial loss of grout from the annulus near the mine roof, could be important to reduce exposure to groundwater, and thus SCC failure of bolts. The findings reported in this study may serve as a basis for future numerical modelling work and analysis of the influence of groundwater and tensile stress in underground coal mines. Also, it can be further used for setting guidelines for the installation of bolts in underground mines to mitigate bolt service failures.

References

Adhikary D, Wilkins A (2012) Reducing the impact of longwall extraction on groundwater systems. CSIRO, Canberra

Allan M (1999) Properties and performance of cement-based grouts for geothermal heat pump applications. Brookhaven National Lab., Upton

Anderson MP, Woessner WW, Hunt RJ (2015) Applied groundwater modeling: simulation of flow and advective transport. Academic Press, Cambridge

Aziz N, Craig P, Nemcik J, Hai F (2014) Rock bolt corrosion—an experimental study. Min Technol 123:69–77

Cao C, Nemcik J, Aziz N, Ren T (2012) Failure modes of rockbolting. 12th Coal Operators' Confernce, University of Wollongong & the Australasian Institute of Mining and Metallurgy 2012:137–153

Chen WF (1982) Plasticity in reinforced concrete. McGraw-Hill, New York

Chen H, Ramandi HL, Walker J, Crosky A, Saydam S (2018) Failure of the threaded region of rockbolts in underground coal mines. Min Technol 127:1–9. https://doi.org/10.1080/14749009.2018.1428060

Coggan J, Gao F, Stead D, Elmo D (2012) Numerical modelling of the effects of weak immediate roof lithology on coal mine roadway stability. Int J Coal Geol 90:100–109

Coli N, Pranzini G, Alfi A, Boerio V (2008) Evaluation of rock-mass permeability tensor and prediction of tunnel inflows by means of geostructural surveys and finite element seepage analysis. Eng Geol 101:174–184

Craig P, Murnane B (2013) In-situ pull testing of cable bolts encapsulated with injection polyurethane. 13th Coal Operators' Conference, University of Wollongong, The Australasian Institute of Mining and Metallurgy & Mine Managers Association of Australia, 2013:131–136.

Craig P, Serkan S, Hagan P, Hebblewhite B, Vandermaat D, Crosky A, Elias E (2016) Investigations into the corrosive environments contributing to premature failure of Australian coal mine rock bolts. Int J Min Sci Technol 26:59–64

Crosky A, Fabjanczyk M, Gray P, Hebblewhite B, Smith B (2002) Premature rock bolt failure. Final report on ARARP Project C8008

Crosky A, Smith B, Hebblewhite B (2003a) Failure of rockbolts in underground mines in Australia. Pract Fail Anal 3:70–78. https://doi.org/10.1007/bf02717427

Crosky A, Smith B, Hebblewhite B (2003b) Failure of rockbolts in underground mines in Australia. J Fail Anal Prev 3:70–78

Day JJ, Diederichs MS, Hutchinson DJ (2017) New direct shear testing protocols and analyses for fractures and healed intrablock rockmass discontinuities. Eng Geol 229:53–72

El Hajj H, Abdelouas A, Grambow B, Martin C, Dion M (2010) Microbial corrosion of P235GH steel under geological conditions. Phys Chem Earth Parts A/B/C 35:248–253

Fredlund DG, Rahardjo H (1993) Soil mechanics for unsaturated soils. Wiley, Hoboken

Gray P (1998) Stress corrosion cracking of rock bolts. In: Aziz, N (ed) Coal 1998: Coal Operators' Conference, University of Wollongong & the Australasian Institute of Mining and Metallurgy, 1998:206–212

Grenon M, Caudal P, Amoushahi S, Turmel D, Locat J (2017) Analysis of a large rock slope failure on the east wall of the LAB chrysotile mine in Canada: back analysis, impact of water infilling and mining activity. Rock Mech Rock Eng 50:403–418. https://doi.org/10.1007/s00603-016-1116-8

Guo H, Yuan L (2015) An integrated approach to study of strata behaviour and gas flow dynamics and its application. Int J Coal Sci Technol 2:12–21. https://doi.org/10.1007/s40789-015-0059-0

Guo PF, Chen QY, Zhang S (2004) Influence analysis of the anchorhold of the resin bolt by the draining water in the drill hole. J China Coal Soc 29:680–683

Guo H, Yuan L, Shen B, Qu Q, Xue J (2012) Mining-induced strata stress changes, fractures and gas flow dynamics in multi-seam longwall mining. Int J Rock Mech Min Sci 54:129–139. https://doi.org/10.1016/j.ijrmms.2012.05.023

Hassell RC (2008) Corrosion of rock reinforcement in underground excavations. Dissertation, Curtin University, 2008.

Hebblewhite B, Lu T (2004) Geomechanical behaviour of laminated, weak coal mine roof strata and the implications for a ground reinforcement strategy. Int J Rock Mech Min Sci 41:147–157

Henthorne M (1971) 1972. A CE refresher series on corrosion causes and control. Chem Eng Mag. A series of 12 articles written between May 17, 1971 through April 3, 1972. Reprinted by Carpenter Technology Reading, Pennsylvania, USA

Heyman J (1972) Coulomb's memoir on statics: an essay in the history of civil engineering. CUP Archive, Cambridge

Hoek E, Brown ET (1980) Underground excavations in rock. CRC Press.

Hyett A, Bawden W, Coulson A (1992) Physical and mechanical properties of normal Portland cement pertaining to fully grouted cable bolts. In: Rock support in mining and underground construction, proceedings of the international symposium rock support. pp 341–348

Inc. R (2017) RS2. www.rocscience.com. Accessed June 2017

Indraratna B, Kaiser P (1990a) Analytical model for the design of grouted rock bolts. Int J Numer Anal Methods Geomech 14:227–251

Indraratna B, Kaiser P (1990b) Design for grouted rock bolts based on the convergence control method. Int J Rock Mech Min Sci Geomech Abstr 4:269–281

Jalalifar H, Aziz N (2012) Numerical simulation of fully grouted rock bolts. In: Andriychuk, M (ed) Numerical simulation: From theory to industry. InTech, pp 607–640

Jing Y, Armstrong RT, Ramandi HL, Mostaghimi P (2017) Topological characterization of fractured coal. J Geophys Res Solid Earth 122:9849–9861. https://doi.org/10.1002/2017jb014667

Kang H (2014) Support technologies for deep and complex roadways in underground coal mines: a review. Int J Coal Sci Technol 1:261–277

Kang H, Wu Y, Gao F, Lin J, Jiang P (2013) Fracture characteristics in rock bolts in underground coal mine roadways. Int J Rock Mech Min Sci 62:105–112

Kelsall PC, Case JB, Chabannes CR (1984) Evaluation of excavation-induced changes in rock permeability. Int J Rock Mech Min Sci Geomech Abstr 21:123–135. https://doi.org/10.1016/0148-9062(84)91530-4

Li L, Hagan PC, Saydam S, Hebblewhite B, Li Y (2016) Parametric study of rockbolt shear behaviour by double shear test. Rock Mech Rock Eng 49:4787–4797. https://doi.org/10.1007/s00603-016-1063-4

Light DD, Donovan JJ (2015) Mine-water flow between contiguous flooded underground coal mines with hydraulically compromised barriers. Environ Eng Geosci 21:147–164

Liu HY, Han H, An HM, Shi JJ (2016) Hybrid finite-discrete element modelling of asperity degradation and gouge grinding during direct shearing of rough rock joints. Int J Coal Sci Technol 3:295–310. https://doi.org/10.1007/s40789-016-0142-1

Ma S, Nemcik J, Aziz N (2014) Simulation of fully grouted rockbolts in underground roadways using FLAC2D. Can Geotech J 51:911–920

Masoumi H, Horne J, Timms W (2017) Establishing empirical relationships for the effects of water content on the mechanical behavior of gosford sandstone. Rock Mech Rock Eng 50:2235–2242

McCafferty E (2010) Introduction to corrosion science. Springer, New York

Mostaghimi P, et al. (2016) Pore scale characterisation of coal: an unconventional challenge. In: Abu Dhabi international petroleum exhibition and conference. Society of Petroleum Engineers

Nemcik J, Ma S, Aziz N, Ren T, Geng X (2014) Numerical modelling of failure propagation in fully grouted rock bolts subjected to tensile load. Int J Rock Mech Min Sci 71:293–300

Newman C, Agioutantis Z, Leon GBJ (2017) Assessment of potential impacts to surface and subsurface water bodies due to longwall mining. Int J Min Sci Technol 27:57–64

Nguyen QP, Manh Nguyen V, Konietzky H, Nguyen QL, Pham NA (2014) Numerical simulation of the influence of water inrush on underground coal mining stability in Vietnam. In: Drebenstedt C, Singhal R (eds) Mine planning and equipment selection. Springer, Cham, pp 629–636

Osouli A, Bajestani BM (2016) The interplay between moisture sensitive roof rocks and roof falls in an Illinois underground coal mine. Comput Geotech 80:152–166

Owen DR, Hinton E (1980) Finite elements in plasticity theory and practice. Pineridge Press

Peng SS (2008) Coal mine ground control. 3rd ed. West Virginia University, Department of Mining Engineering, Morgantown, WV (USA)

Perras MA, Diederichs M (2007) Engineering geology, glacial preconditioning, and rockmass response to large scale underground excavations in the Niagara Region. In: 1st Canada-US rock mechanics symposium. American Rock Mechanics Association

Pittman ED (1992) Relationship of porosity and permeability to various parameters derived from mercury injection-capillary pressure curves for sandstone (1). AAPG Bull 76:191–198

Potvin Y, Nedin P, Sandy M, Rosengren K, Rosengren M (2001) Towards the elimination of rockfall and fatalities in Australian mines. Government of Western Australia

Ramandi HL, Mostaghimi P, Armstrong RT (2016) Digital rock analysis for accurate prediction of fractured media permeability. J Hydrol. https://doi.org/10.1016/j.jhydrol.2016.08.029

Ramandi HL, Chen H, Crosky A, Saydam S (2018a) Interactions of stress corrosion cracks in cold drawn pearlitic steel wires: an X-ray micro-computed tomography study. Corros Sci 145:170–179. https://doi.org/10.1016/j.corsci.2018.09.009

Ramandi HL, Liu M, Tadbiri S, Mostaghimi P (2018b) Impact of dissolution of syngenetic and epigenetic minerals on coal permeability. Chem Geol. https://doi.org/10.1016/j.chemgeo.2018.03.015

Sasaoka T, Karian T, Hamanaka A, Shimada H, Matsui K (2016) Application of highwall mining system in weak geological condition. Int J Coal Sci Technol 3:311–321. https://doi.org/10.1007/s40789-016-0121-6

Smith JV (2016) Assessing the ability of rock masses to support block breakage at the TBM cutter face. Tunn Undergr Space Technol 57:91–98

Snow DT (1968) Rock fracture spacings, openings, and porosities. J Soil Mech Found Div 94(1):73–92

Spearing A, Mondal K, Bylapudi G, Hirschi J (2010) The corrosion of rock anchors in US coal mines. In: Proceedings of the SME annual meeting, Phoenix, AZ, USA

Surinaidu L, Rao VG, Rao NS, Srinu S (2014) Hydrogeological and groundwater modeling studies to estimate the groundwater inflows into the coal mines at different mine development stages using MODFLOW, Andhra Pradesh, India. Water Resour Ind 7:49–65

Tepfers R (1973) A theory of bond applied to overlapped tensile reinforcement splices for deformed bars. Chalmers University of Technology, Göteborg

Tepfers R (1979) Cracking of concrete cover along anchored deformed reinforcing bars. Mag Concr Res 31:3–12

Vandermaat D (2015) Stress corrosion cracking of rockbolts: a laboratory based approach utilising a controlled mine environment. UNSW Australia, Sydney, Australia (PhD. Thesis)

Vandermaat D, Saydam S, Hagan PC, Crosky AG (2016) Examination of rockbolt stress corrosion cracking utilising full size rockbolts in a controlled mine environment. Int J Rock Mech Min Sci 81:86–95

Wang JA, Park HD (2002) Fluid permeability of sedimentary rocks in a complete stress–strain process. Eng Geol 63:291–300. https://doi.org/10.1016/s0013-7952(01)00088-6

Wang J, Yu B, Kang H, Wang G, Mao D, Liang Y, Jiang P (2015) Key technologies and equipment for a fully mechanized top-coal caving operation with a large mining height at ultra-thick coal seams. Int J Coal Sci Technol 2:97–161. https://doi.org/10.1007/s40789-015-0071-4

Windsor C (1997) Rock reinforcement systems. Int J Rock Mech Min Sci 34:919–951

Winn K, Ng M, Wong LNY (2017) Stability analysis of underground storage cavern excavation in Singapore. Procedia Eng 191:1040–1047. https://doi.org/10.1016/j.proeng.2017.05.277

Wong P-z, Koplik J, Tomanic J (1984) Conductivity and permeability of rocks. Phys Rev B 30:6606

Wu S et al (2018a) An experimental framework for simulating stress corrosion cracking in cable bolts. Tunn Undergr Space Technol 76:121–132. https://doi.org/10.1016/j.tust.2018.03.004

Wu S, Chen H, Ramandi HL, Hagan PC, Hebblewhite B, Crosky A, Saydam S (2018b) Investigation of cable bolts for stress corrosion cracking failure. Constr Build Mater 187:1224–1231. https://doi.org/10.1016/j.conbuildmat.2018.08.066

Wu S, Chen H, Ramandi HL, Hagan PC, Crosky A, Saydam S (2018c) Effects of environmental factors on stress corrosion cracking of cold-drawn high-carbon steel wires. Corros Sci 132:234–243. https://doi.org/10.1016/j.corsci.2017.12.014

Wu S, Northover M, Craig P, Canbulat I, Hagan PC, Saydam S (2018d) Environmental influence on mesh corrosion in underground coal mines. Int J Min Reclam Environ 32:519–535

Yassien AM (2003) 2-D numerical simulation and design of fully grouted bolts for underground coal mines. West Virginia University Libraries, Morgantown

Zhang C, Mitra R, Hebblewhite B (2012) Review of numerical modelling evaluation of mechanisms for valley closure subsidence under irregular topographic condition. In: ISRM international symposium-EUROCK 2012. International Society for Rock Mechanics

Zsaki A (2010) Optimized mesh generation for two-dimensional finite element analysis of underground excavations in rocks masses traversed by joints. Int J Rock Mech Min Sci 47:553–558